15th IFK
Proc. of the 15th International Fluid Power Conference <Symposium/Conference>
<DOI>

Hydraulic Artificial Muscles for Exoskeleton Actuation Solutions

Mathias Niebergall, Jonas Pfister, Roman Strobel, Jonathan Scheible

Mathias.Niebergall@thu.de, Jonas.Pfister@thu.de , Roman.Strobel@thu.de , Jonathan.Scheible@thu.de

Abstract

Exoskeletons are designed to enhance the human physical capabilities and to reduce physical strain for various applications in terms of e. g. medical rehabilitation, every day assistance or physical working performance. The actuation of active exoskeletons by means of hydraulic artificial muscles (McKibben principle) are convincing solutions due to their light weight, compactness, exceptional power capacity, remarkable resiliency, and low investment costs. [1] The artificial muscle presented comprises an inner elastomeric hose surrounded by a textile, braided and reinforced by aramid fibers. The muscle is activated by hydraulic fluid supply that cause a radial expansion of the inner pressurized hose and a corresponding axial contraction of the muscle as actuation effect [2], [3], [4], [5], [6], [7], [8]. This paper presents a mathematical-physical model of the hydraulic artificial muscle based on conservation of mass and conservation of energy. Prototypes of hydraulic artificial muscles have been developed for selected drive functions and experimentally tested.
Based on [9] a hydraulic muscle with a length (without fittings) of 200 mm and with an inner diameter (elastomer tube) of 6 mm and an outer diameter of ca. 10 mm (elastomer tube + fiber fabric) has been experimentally evaluated. Relating to the initial length of the hydraulic muscle a contraction of up to 32 % is reachable. With a pressure level of 10 MPa an advanced force density per mass of 110 kN/kg of the muscle is now accessible.
Due to its flexible structure, a hydraulic muscle is much more compliant and adaptable than a rigid hydraulic cylinder. This makes the muscle design ideal for wearable actuation systems. Additionally, the muscle is hermetically sealed, due to its closed design.
An exoskeleton test setup has been developed for experimental investigations. The paper finally discus hydraulic muscles for exoskeleton drive functions.

Keywords Hydraulic Artificial Muscle, Mathematical-Physical Modeling, High Pressure Actuation, Exoskeleton Drive

1. INTRODUCTION

New innovative actuator systems for exoskeletons with hydraulic artificial muscles are very attractive solutions due to their remarkable compactness, lightweight, robustness, and low investment costs. Various prototypes of hydraulic artificial muscles have been developed and built. A sectional view of a typical prototype is shown in Figure 1.1. The muscle has an inner elastomeric hose, surrounded by an aramid fiber textile sleeve, at both ends equipped with a typical hydraulic hose fitting. The fitting composed of a swage nipple and a swage ferrule, as well as a screw coupling with an O-ring sealing element.

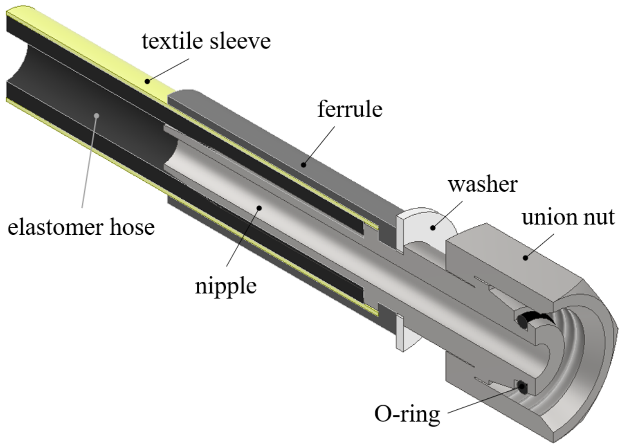

Figure 1.1 Sectional view of the hydraulic artificial muscle [9]

This publication focuses on the following topics:

- introduction of a quasi-static theoretical model of the hydraulic muscle (chapter 2)
- description of the experimental test set up (section 3.1)
- experimental investigations on hydraulic artificial muscles with three muscle length and two muscle diameters for the verification of the model equations (section 3.2)
- experimental high-pressure test (10 MPa) to determine the high force density of a hydraulic artificial muscle (chapter 4)
- an exoskeleton application solution for hydraulic artificial muscles (chapter 5)

The contraction of the hydraulic artificial muscle is illustrated schematically in Figure 1.2. Fluid supply activates the initially non-pressurized muscle with the radius R_0, the initial length L_0 and the fiber angle α_0 (compare Figure 1.3). The pressurized hose surface leads to radial hydraulic forces with increasing circumferential stress in the surrounding textile reinforcement sleeve. With radial displacement of the inner pressurized bladder over the whole length of the muscle, the fiber angle and the radius increases up to α_1 and R_1 respectively. The corresponding axial contraction of the hydraulic artificial muscle to the length L_1 is the actuation effect.

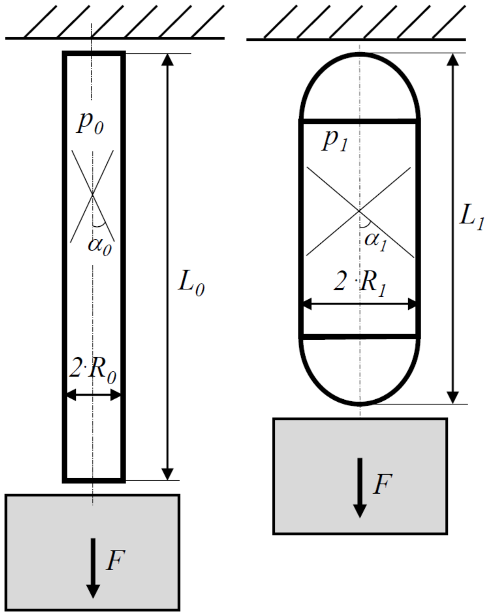

Figure 1.2 Sketch of the simplified non-pressurized muscle (left) and the pressurized activated muscle (right)

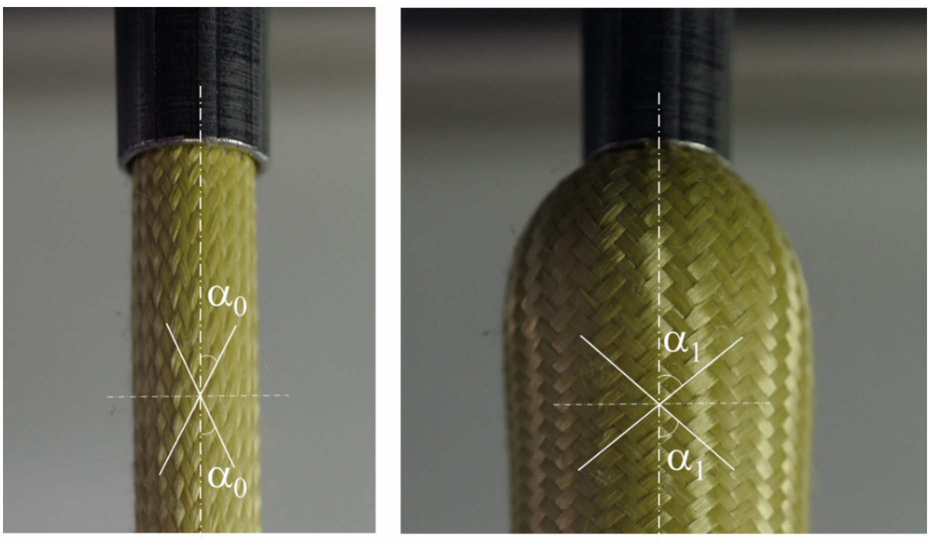

Figure 1.3 Fiber angle of a non-pressurized muscle α_0 and of a pressurized muscle α_1 [9]

2. STATIC MODEL OF HYDRAULIC ARTIFICIAL MUSCLES

In the last decades fluidic (pneumatic or hydraulic) artificial muscles have been investigated and discussed in several studies (e. g. Schulte (1961) [2], Chou, Hannaford (1996) [3], Tondu and Lopez (2000) [4], Tiwari, Meller et al. (2012) [5], Pan et al. (2020) [6], Mori, Suzumori (2009) [7], Zhang et al. (2022) [8]).

The physical approaches for fluidic artificial muscles are typically based on energy conservation, virtual work principles, and on a simplified cylindrical geometry. In general, the fluidic work is done by increasing the volume of the muscle, and leads finally to the mechanical work, done by the muscle as it contracts and changes length. [5]

For the below-described mathematical-physical modeling of the hydraulic artificial muscle, following assumptions are taken into account:

- quasi-static consideration of the actuation process
- compressible muscle including elastomer hose, textile sleeve and fluid
- homogeneously distributed volume flow q
- constant change in constant homogeneously distributed density of the fluid ρ
- cylindrical tube shape (the volume around the end cap sphere (compare Figures 1.2 and 1.3) will be later subtracted)

Initially an artificial muscle approach to mass conservation has been derived and subsequently the relationship to energy conservation is discussed.

Conservation of mass.

The continuity equation (2.1) has here the following components:

- the mass flow supplied to the hydraulic muscle (inflow),
- the mass flow of displacement of the muscle (deformation), and
- the mass flow of elasticity behaviour of the muscle (compression),

$$\underbrace{\rho \cdot q}_{inflow} + \underbrace{\rho \cdot \frac{d}{dt} \cdot \int_V dV}_{deformation} + \underbrace{\rho \cdot \frac{1}{\kappa} \cdot \dot{p} \cdot \int_V dV}_{compression} = 0 \tag{2.1}$$

with the mass density of the fluid ρ, the flow rate into the muscle q, the change of the muscle volume dV, the compression number of the muscle κ, and the change of pressure dp/dt. The compression number κ indicates the pressure required for the elastic muscle deformation.

The balance of volume flow, in case of equal density of the fluid, is shown in equation (2.2), which takes into account the inflow rates (+) and outflow rates (-) via the signs.

$$q - \frac{d}{dt} \cdot \int_V dV - \frac{1}{\kappa} \cdot \dot{p} \cdot \int_V dV = 0 \tag{2.2}$$

Integration over time from the initial state at t_0 to the final contraction state at t_1 yield to the equation of the volumes (2.3).

$$\int_{t_0}^{t_1} q \, dt - \int_V dV - \frac{p}{\kappa} \cdot \int_V dV = 0 \tag{2.3}$$

The change of the muscle volume dV can be described by infinitesimal steps of the two main influencing variables: the radius of the muscle R and the length of the muscle L (compare Figure 1.2 and equation (2.4)).

$$dV = \left(\frac{\partial V}{\partial R}\right)_{L_0} \cdot dR + \left(\frac{\partial V}{\partial L}\right)_{R_1} \cdot dL \tag{2.4}$$

The partial derivatives of (2.5a) are (2.5b) and (2.5c).

$$V = R^2 \cdot \pi \cdot L \tag{2.5a}$$

$$\left(\frac{\partial V}{\partial R}\right) = 2 \cdot R \cdot \pi \cdot L \tag{2.5b}$$ $$\left(\frac{\partial V}{\partial L}\right) = R^2 \cdot \pi \tag{2.5c}$$

Integration of (2.4) leads to the deformation relationship (2.6) with respect to the state limits (R_1, L_1) of the actuated muscle (compare Figure 1.2).

$$V = \int dV = \int_{R_0}^{R_1} \left(\frac{\partial V}{\partial R}\right)_{L_0} \cdot dR + \int_{L_0}^{L_1} \left(\frac{\partial V}{\partial L}\right)_{R_1} \cdot dL \tag{2.6}$$

The solution is the volume of muscle deformation (2.7). Here the term V_1 represents the radial expanded and contracted volume, and the term V_0 the initial volume of the muscle.

$$V = \underbrace{R_1^2 \cdot \pi \cdot L_1}_{V_1} - \underbrace{R_0^2 \cdot \pi \cdot L_0}_{V_0} \tag{2.7}$$

Based on (2.3) and (2.7) equation (2.8) describes the proportions of the change in volume of the artificial muscle.

$$\int_{t_0}^{t_1} q \, dt - \left(R_1^2 \cdot \pi \cdot L_1 - R_0^2 \cdot \pi \cdot L_0\right) - \chi \cdot \left(R_1^2 \cdot \pi \cdot L_1 - R_0^2 \cdot \pi \cdot L_0\right) = 0 \tag{2.8}$$

with the compression factor $\chi = p / \kappa$ as dimensionless parameter that describes the average compliance during the muscle actuation.

Conservation of energy.

The energy conservation of hydraulic artificial muscles (2.9) follows from the inclusion of pressure in equation (2.8).

$$\underbrace{\int_{t_0}^{t_1} q \cdot p \, dt}_{supply} - \underbrace{\left(R_1^2 \cdot \pi \cdot L_1 - R_0^2 \cdot \pi \cdot L_0\right) \cdot p}_{deformation\,/\,actuation} - \underbrace{\chi \cdot \left(R_1^2 \cdot \pi \cdot L_1 - R_0^2 \cdot \pi \cdot L_0\right) \cdot p}_{elastic\ deformation} = 0 \quad (2.9)$$

In the literature (e. g. [2], [3], [4], [5], [6], [7], [8]), deformation energy is equated with the mechanical work of displacement in the form (2.10a), that lead here to equation (2.10b).

$$-\int_{L_0}^{L_1} F \, dL = \int_{V_0}^{V_1} p \, dV \quad (2.10a), \qquad -\int_{L_0}^{L_1} F \, dL = p \cdot (R_1^2 \cdot \pi \cdot L_1 - R_0^2 \cdot \pi \cdot L_0) \quad (2.10b)$$

The second term of the displacement work in equation (2.11) replaces the muscle deformation term in (2.9). Thus, the conservation of energy approach has the following form:

$$\int_{t_0}^{t_1} q \cdot p \, dt - \int_{L_1}^{L_0} F \, dL - \chi \cdot \left(R_1^2 \cdot \pi \cdot L_1 - R_0^2 \cdot \pi \cdot L_0\right) \cdot p = 0 \quad (2.11)$$

Due to the rounding of the end caps after the muscle contraction (compare Figure 1.2), equation (2.11) can be corrected by taking the V_R volume (2.12) into account.

$$V_R = \underbrace{R_1^2 \cdot \pi \cdot 2 \cdot R_1}_{cylinder} - \underbrace{\frac{4}{3} \cdot R_1^3 \cdot \pi}_{sphere} \quad (2.12)$$

Then the conservation of energy approach for hydraulic artificial muscles has finally the following form (2.13):

$$\underbrace{\int_{t_0}^{t_1} q \cdot p \, dt}_{supply\,(E_s)} - \underbrace{\int_{L_1}^{L_0} F \, dL}_{actuation\,(W)} - \underbrace{\chi \cdot \left(R_1^2 \cdot \pi \cdot L_1 - V_R - R_0^2 \cdot \pi \cdot L_0\right) \cdot p}_{elastic\ deformation\,(E_e)} = 0 \quad (2.13)$$

The energy conservation approach (2.13) contains the hydraulic energy supply E_s to the muscle, the mechanical work W done and the energy share of the elastic compression / energy storage (and where appropriate energy losses) E_e of the muscle. For the verification of the energy balance (2.13) the mechanical work W, the energy supplied E_s and the Energy of the elastic compression E_e are experimentally determined and presented in the following chapter 3.

The compression factor $\chi = p_m / \kappa$ is a dimensionless parameter that describes the average compliance during muscle deformation, by means of

- the average measured pressure p_m during the muscle contraction, and
- the compression number κ, that indicates the average pressure required for muscle contraction, dependent on the muscle geometry.

Here the compression factor χ was determined using equation (2.13), rearranged according to the compression factor when all other data were available as measured data (compare section 3.2). Due to the experimental determination of χ, it also includes the energy losses (in case of relevance) during the contraction of the artificial muscle.

3. Experimental Analysis of Hydraulic Artificial Muscles

The experimental investigations of the artificial muscles and the verification of the model equations (2.13) have been carried out with an appropriate test setup. The experimental equipment is presented in section 3.1 and the test results are discussed in section 3.2.

3.1. Description of the experimental equipment

The test setup for hydraulic artificial muscles is shown schematically in Figure 3.1 and the test chamber of the test setup is shown in Figure 3.2 as photography.
The hydraulic artificial muscle (1) is suspended in the test chamber and loaded with a defined weight (8). The muscle is activated by a volume flow of a pressure fluid (mineral oil) from a hydraulic power unit (2). The muscle contraction is controlled by means of a 4/3-way valve.

The functional tests of the artificial muscle are monitored by measurement technology using the following components:

- pressure sensors (5) for monitoring the pressure load of the muscle,
- flow rate sensor (3) for measuring the volume flow into the muscle,
- force sensor (4) for monitoring the quasi-static load,
- laser distance sensor (7) for detecting the muscle contraction,
- displacement sensors (6) for the measurement of the muscle diameter,
- camera (9) for visual recording the changing fiber angle of the textile shell, and
- amplifier (10) for recording and logging the measurement data.

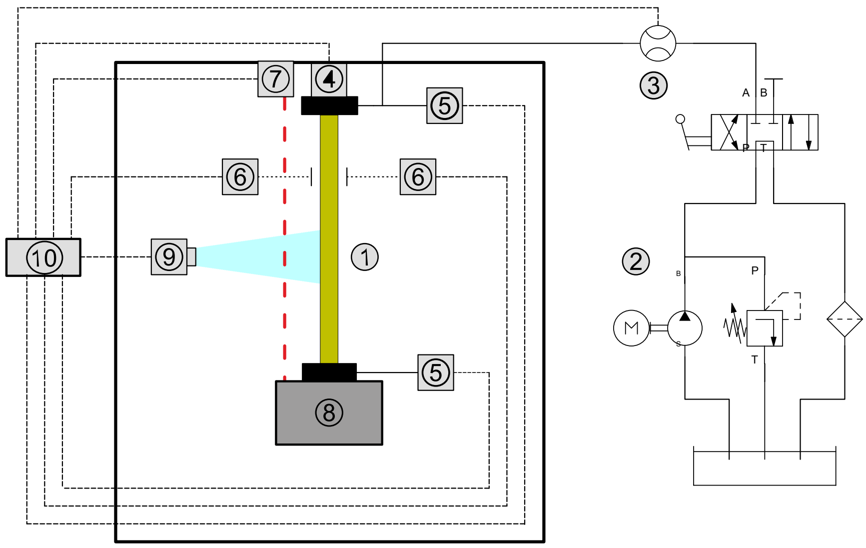

Figure 3.1 Schematic representation of the test setup with hydraulic test environment (dashed lines denote electrical signal lines)

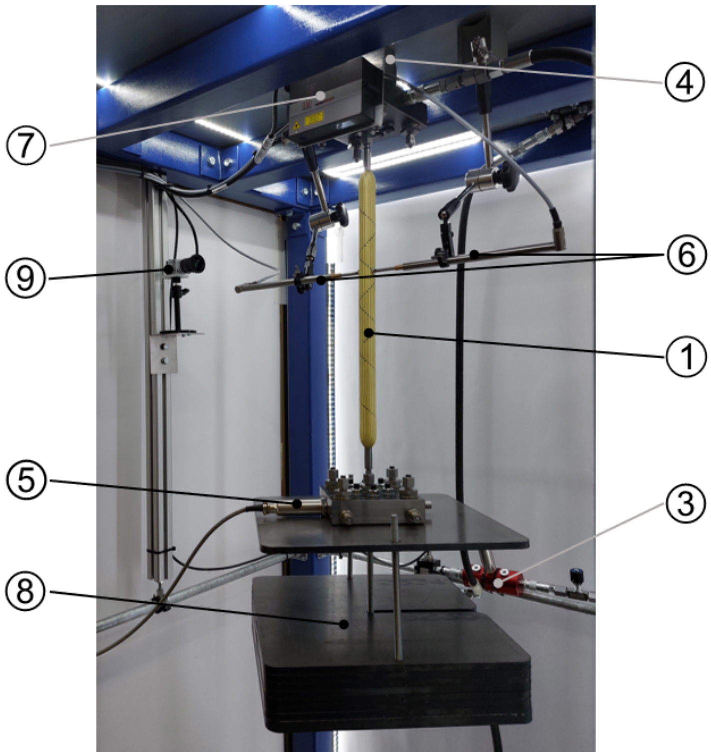

Figure 3.2 Photo of the test setup for experimental investigations of hydraulic artificial muscles (here exemplarily a pressurized muscle (1) with a length of 0.6 m and 100 kg load)

3.2. Experimental investigations of the hydraulic artificial muscle

Non-pressurized hydraulic artificial muscles with three different initial lengths L_0 of 0.3 m, 0.45 m and 0.6 m and with two different initial outer diameters D_0 of 8 mm and 10 mm have been configured for muscle tests. The artificial muscles have been activated by a volume flow q with an increase of the corresponding pressure p up to 5 MPa. The actuation effect is the contraction of the artificial muscles caused by a quasi-static load of 310.8 N for the D08-muscle (D_0 = 8 mm, α_0 = 24°) or 993.6 N for the D10-muscle (D_0 = 10 mm, α_0 = 17°) respectively. The pressurized artificial muscles have an expansion of the outer diameter to D_1 (α_1 = 44° for the D08-muscle, α_1 = 48° for the D10-muscle) and they are shortened to the respective length L_1. Relating to the initial length L_0 of the non-pressurized muscles, and the measured length changes (L_0 - L_1), the contractions ε can be calculated with equation (3.1).

$$\varepsilon = \frac{L_0 - L_1}{L_0} \cdot 100\% \tag{3.1}$$

The experimental initial data (L_0, $D_0 = 2\,R_0$ and F), the measured test results in the contracted state of the muscle (L_1, R_1), and the calculated test results from measured data (ε, κ, χ, E_s, W, E_e) are summarized in Table 3.1. The contraction ε of the artificial muscle show a dependence on the muscle diameter and on the load force. The compression number κ for the contraction of the artificial muscle show a dependence to the muscle length.

The associated measurement results are shown exemplary for the D10-muscles with their three initial lengths (0.3 / 0.45 / 0.6 m) in Figure 3.3. The calculated energy shares, based on equation (2.13), associated to the measurement results, are shown in Figure 3.4. The energy supplied for muscle contraction E_s corresponds to the sum of mechanical work W and elastic energy E_e, due to the compression number κ (or factor χ).

Table 3.1 Measurement data and calculation results of the initial state ($_0$) and the contracted state ($_1$) of the tested hydraulic artificial muscles

	D08 - muscle			D10 - muscle			unit
initial muscle length L_0	0.3	0.45	0.6	0.3	0.45	0.6	m
initial outer diameter D_0	8	8	8	10	10	10	mm
load force F	310.8	310.8	310.8	993.6	993.6	993.6	N
muscle length L_1 (5 MPa)	0.2405	0.3582	0.4804	0.2211	0.3280	0.4443	m
inner radius R_1 (5 MPa)	5.1	5.3	5.2	11.6	11.8	11.6	mm
contraction ε (5 MPa)	20.9	20.9	21.3	27.0	27.6	26.8	%
compression number κ	0.80	1.44	2.09	4.20	4.84	5.30	MPa
compression factor χ	1.56	1.00	0.78	0.342	0.307	0.301	-
supplied energy E_s	53.59	70.33	86.34	121.21	182.52	241.48	J
mechanical Work W	19.75	29.47	40.29	81.40	124.23	161.66	J
elastic energy E_e	33.84	40.85	46.05	39.82	58.29	79.82	J

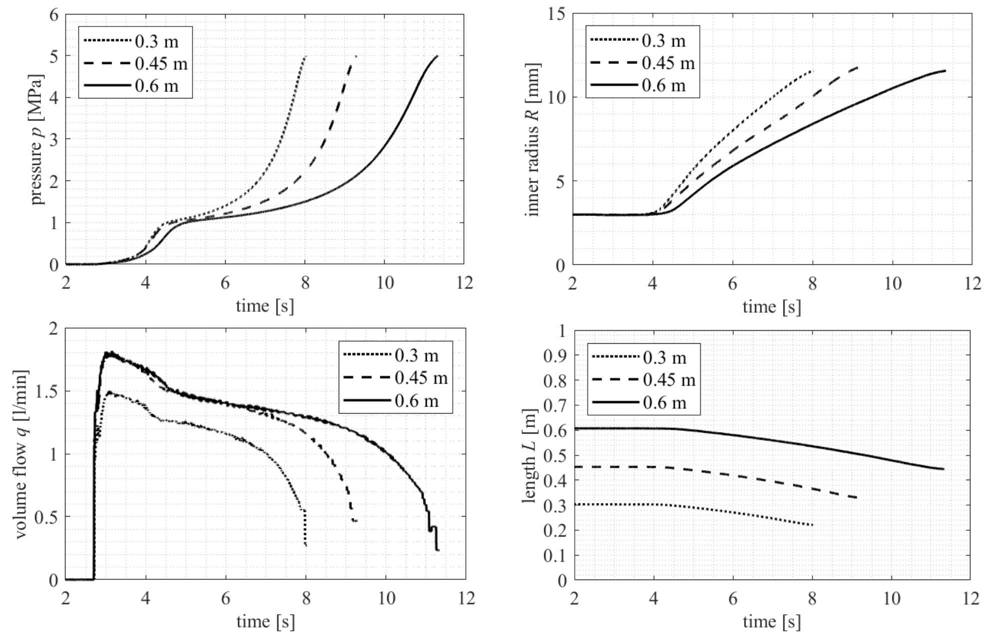

Figure 3.3 Measured test results of pressure p, flow rate q, muscle diameter D and muscle length L for the hydraulic artificial D10-muscles of the initial lengths $L_0 = 0.3 / 0.45 / 0.6$ m

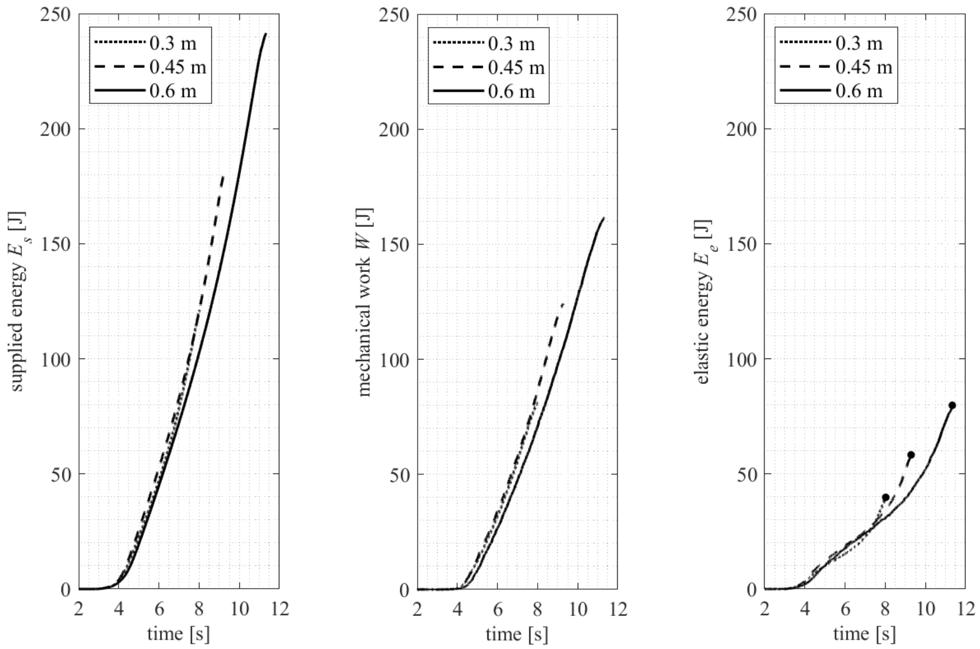

Figure 3.4 Energy conservation shares (compare equation (2.13)) for the hydraulic artificial D10-muscles of different length based on the measured data of Figure 3.3

4. Artificial Muscles with High Force Density

For the investigation of the maximum force performance as well as the force density of the artificial muscle a hydraulic test setup has been developed, that is shown in Figure 4.1 with the measuring equipment. Here the muscle has to be clamped within the test setup to prevent its axial contraction during the recording of the blocked force. The muscle has an initial length of $L_0 = 200$ mm, a diameter $D_0 = 10$ mm, and a mass including fittings and filled with fluid of $m = 0{,}120$ kg. The measured force characteristic curve dependent on pressure of the blocked muscle is shown in Figure 4.2. Because of the clamping the blocked force rises with increasing pressure up to a high pressure of 10 MPa and a force level of $F_t = 14200$ N. Calculated with (4.1), the force density per mass of the muscle is $\delta_F = 110$ kN/kg.

$$\delta_F = \frac{F_t}{m} \tag{4.1}$$

The improvement in power density is based on a significantly higher pressure level (10 MPa) compared to 5.6 MPa in [9] due to improved form-fit connection between muscle and fitting.

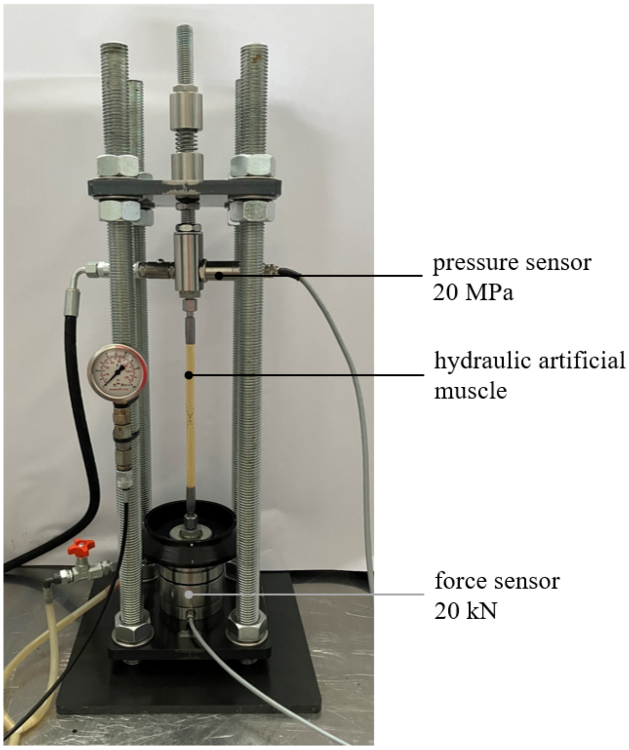

Figure 4.1 Test setup for determining the force density of hydraulic artificial muscles

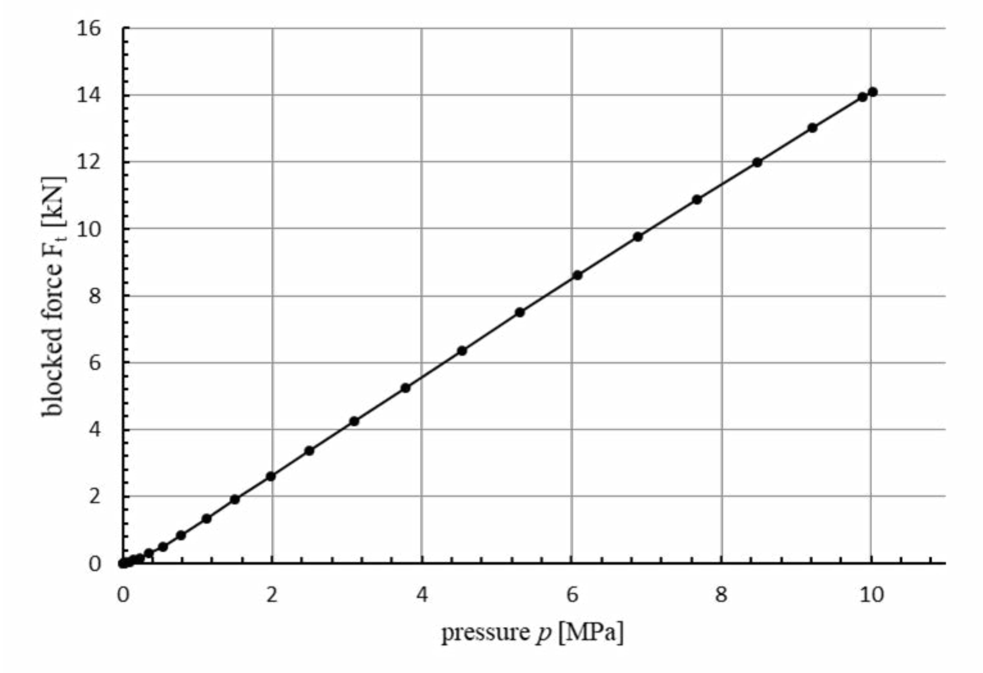

Figure 4.2 Measured blocked force of the clamped muscle in Figure 4.1

5. Hydraulic Exoskeleton Applications

Hydraulic artificial muscles are much more compliant and adaptable, due to their high force density advantages as well as because of their flexible textile braided structure compared to rigid electromechanical drives or conventional hydraulic cylinders. The muscles are hermetically sealed, due to the closed design using elastomeric hoses. For these reasons, the hydraulic artificial muscles are ideally suited for wearable actuation systems. For experimental investigations, an exoskeleton test setup has been built that enables the testing of selected exoskeleton drive functions as shown in Figure 5.1.

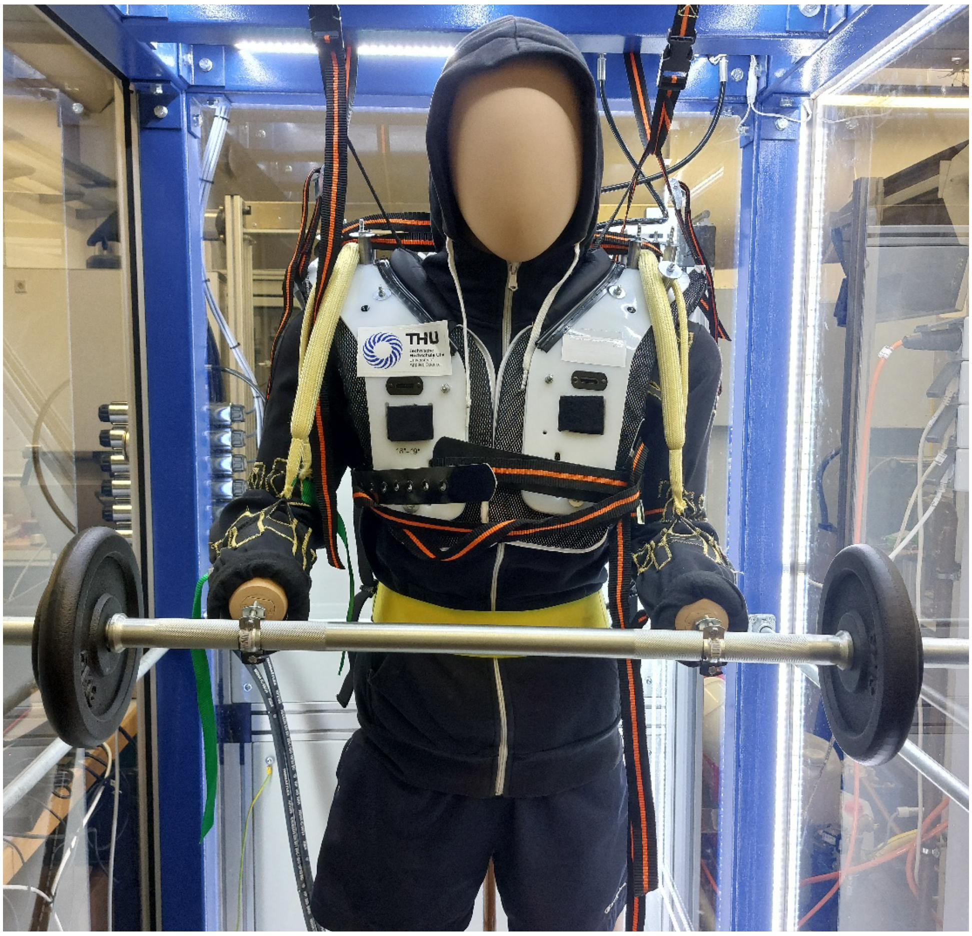

Figure 5.1 Exoskeleton test setup for power support for the upper body (here 20 kg)

6. CONCLUSION

The actuation of active exoskeletons by means of hydraulic artificial muscles are convincing solutions, due to their light weight, compactness, exceptional power capacity, remarkable resiliency, and low investment costs.

A mathematical-physical model of hydraulic artificial muscles is initially presented, based on an approach of conservation of mass and conservation of energy (chapter 2). For the test of the model equations, hydraulic artificial muscles with three different initial length and two initial diameters have been prepared and experimentally investigated. The experimental results confirm the model equations, taking into account adjusted compression factors that describe the elasticity or the energy storage capacity of the muscle (chapter 3).

With a further experiment the maximum blocked force of a hydraulic artificial muscle (length 200 mm, diameter 10 mm) under high pressure requirements of 10 MPa has been determined. It results in a measured blocked force of 14200 N with a very competitive force density per mass of δ_F = 110 kN/kg (muscle mass m = 0,120 kg) (chapter 4).

An exoskeleton test setup has been built for experimental investigations that enables the testing for selected exoskeleton drive functions. These investigations demonstrate that hydraulic artificial muscles are much more compliant and adaptable, due to their high force density advantages as well as due to their flexible textile braided structure compared to rigid electromechanical solutions or conventional hydraulic cylinders. The closed muscle design using elastomeric hoses enables a hermetically sealing.

In summary, the hydraulic artificial muscles are ideally suited for wearable exoskeleton actuation systems (chapter 5).

Acknowledgement

The authors would like to thank the foundation council of the Hydraulics Center of Excellence of the Ulm University of Applied Sciences for the friendly support of the project.

7. REFERENCES

[1] D. M. G. Preethichandra, L. Piyathilaka et al., Passive and Active Exoskeleton Solutions: Sensors, Actuators, Applications, and Recent Trends, in: Sensors 2024, 24, 7095, 2024

[2] H.F. Schulte, The characteristics of the McKibben artificial muscle, The Application of External Power in Prosthetics and Orthotics, Washington, DC: Nat. Acad. Sci.-Nat. Res. Council, 1961

[3] C.-P. Chou, B. Hannaford, Measurement and Modeling of McKibben Pneumatic Artificial Muscles, IEEE Transactions on Robotics and Automation, Vol. 12, No. 1, 1996

[4] B. Tondu, P. Lopez, Modeling and Control of McKibben Artificial Muscle Robot Actuators, IEEE Control Systems Magazine, 20 (2): 15-38, 2000

[5] R. Tiwari, M. A. Meller, Hydraulic Artificial Muscles, Journal of Intelligent Material Systems and Structures, 23(3) 301-312, 2012

[6] M. Pan, Zhe Hao, Chenggang Yuan, Andrew Plummer, Development and Control of Smart Pneumatic McKibben Muscles for Soft Robots, in: 12th International Fluid Power Conference, 2020

[7] M. Mori, K. Suzumori, S. Seita, M. Takahashi, T. Hooya, K. Kusumoto, Development of Very High Force Hydraulic McKibben Artificial Muscle and Its Application to Shape-Adaptable Power Hand, Proceedings of the IEEE International Conference on Robotics and Biomimetics, 2009

[8] Z. Zhang, J. Che, P. Liu, Y. Jia, Y. Gong, A Modified Physical Model of High-Strength Water Hydraulic Artificial Muscles Considering the Effects of Geometry and Material Properties, Journal of Mechanical Engineering Science, Vol. 236 (2), 2022

[9] M. Niebergall, R. Strobel, Development of a hydraulic artificial muscle with high force density, in: 14th International Fluid Power Conference, Dresden 2024, pp. 94 – 103, 2024

Biographies

Mathias Niebergall received the master's degree in 1990 and his doctorate in mechanical Engineering in 1996 from the University of Kassel. After working in industry with Bosch and Bosch Rexroth, he is since 2014 Professor at the Ulm University of Applied Science (THU) at the Department of Mechanical and Automotive Engineering. His research focuses on hydraulic drive systems.

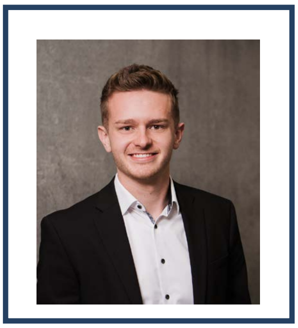

Jonas Pfister holds a bachelor's degree in automotive Engineering and is currently studying for a master's degree in Systems Engineering at Ulm University of Applied Science. In addition to his studies, he works at the Hydraulics Center of Excellence at the THU.

Roman Strobel received the master's degree in Systems Engineering at Ulm University of Applied Science. In addition to his employment in industry, he works at the Hydraulics Center of Excellence at the THU.

Jonathan Scheible holds a bachelor's degree in automotive engineering. In addition to his employment in industry, he works at the Hydraulics Center of Excellence at the THU.